SCIENTIFIC REPORTS

OPEN

SUBJECT AREAS:
INFORMATION STORAGE
ELECTRONIC DEVICES
APPLIED PHYSICS
ELECTRONIC PROPERTIES AND MATERIALS

Received
4 January 2013

Accepted
8 April 2013

Published
23 April 2013

Correspondence and requests for materials should be addressed to H.-H.P. (hhpark@yonsei.ac.kr) or M.J.R. (rozenberg@lps.u-psud.fr)

# A new route to the Mott-Hubbard metal-insulator transition: Strong correlations effects in $Pr_{0.7}Ca_{0.3}MnO_3$

Hong Sub Lee[1], Sun Gyu Choi[1], Hyung-Ho Park[1] & M. J. Rozenberg[2,3]

[1]Department of Materials Science and Engineering, Yonsei University, Seodaemun-Ku, Seoul 120-749, Korea, [2]Laboratoire de Physique des Solides, CNRS-UMR 8502 Université Paris-Sud, Orsay 91405, France, [3]Departamento de Física, FCEN, Universidad de Buenos Aires, Ciudad Universitaria Pabellón I, (1428) Buenos Aires, Argentina.

**Resistive random access memory based on the resistive switching phenomenon is emerging as a strong candidate for next generation non-volatile memory. So far, the resistive switching effect has been observed in many transition metal oxides, including strongly correlated ones, such as, cuprate superconductors, colossal magnetoresistant manganites and Mott insulators. However, up to now, no clear evidence of the possible relevance of strong correlation effects in the mechanism of resistive switching has been reported. Here, we study $Pr_{0.7}Ca_{0.3}MnO_3$, which shows bipolar resistive switching. Performing micro-spectroscopic studies on its bare surface we are able to track the systematic electronic structure changes in both, the low and high resistance state. We find that a large change in the electronic conductance is due to field-induced oxygen vacancies, which drives a Mott metal-insulator transition at the surface. Our study demonstrates that strong correlation effects may be incorporated to the realm of the emerging oxide electronics.**

Resistive random access memory (ReRAM) is considered a promising candidate for next generation non-volatile memory due to its simple metal/insulator/metal (MIM) structure, fast read/write speed, and possibility of realizing cross-point array structures. So far, a variety of resistive switching characteristics were observed in MIM structures using a transition metal oxide as dielectric, and various mechanisms were suggested[1–9]. Among the many candidate materials for ReRAM, the strongly correlated electron system $Pr_{0.7}Ca_{0.3}MnO_3$ (PCMO), that belongs to the family of perovskite manganites $R_{1-x}A_xMnO_3$ ($R$ = rare-earth metal; $A$ = divalent element), has received a great deal of attention. The reason is that, despite its complex stoichiometry, it shows bipolar resistive switching (RS) without the need of a "forming process", in contrast to the simpler binary transition metal oxide systems. In fact, PCMO has been continuously studied for applications of ReRAM since the initial discovery of the resistive switching phenomenon[1]. In transition metal oxides, the extra holes/electrons are doped at either the transition metal or the oxygen atom, depending on whether the oxide has an early or late transition metal[10,11]. In PCMO, Pr and Ca outer electrons are transferred to the oxygen atom to complete the O 2p shell. Therefore, excess holes/electrons are primarily located in Mn 3d by $Ca^{2+}$ doping, which thus controls the Mn 3d filling. The schematic electronic structure that emerges for the compound series $Pr_{1-x}Ca_xMnO_3$ is that the Mn 3d $e_g$ band is singly occupied, with one electron per site, for x= 0, and is progressively depleted with the increase of the Ca concentration x, with complete depletion for x= 1. The band picture is therefore consistent with the fact that both end members are insulators (Mott-charge-transfer or band insulators, respectively for x= 0 or 1). One might naively expect metallic states for the intermediate compounds, however they actually are correlated semiconductors. While they have activated resistivity, they also show anomalous behavior such as, for instance, large (negative) magnetoresistance[12]. The full understanding of the electronic structure and conduction properties of PCMO remains a challenging problem of strongly correlated systems[12–14].

The phenomenology of the observed resistive switching characteristics of oxides for ReRAM applications is currently classified as of unipolar or bipolar type[1,3]. In the former, the origin of the mechanism is discussed in terms of a "filament model"[15], where a thin metallic filament is created by soft dielectric breakdown and then burnt like a fuse. On the other hand, in the bipolar case the effect is associated to an interface and various possible mechanisms have been suggested, such as a redox of top electrode (TE)[16], change of Schottky-like barrier with electrochemical migration[3,6], redox of Metal-O-Metal conduction chain[9], Mott Hubbard metal-insulator transition (MIT)[7], etc. These mechanisms were proposed following a variety of experimental observations, such as the

relationship between oxygen vacancy concentration and high-low resistance ratio $R_H/R_L$, electrode-element dependence, and dependence of I–V characteristics with polarity[3,6,17–19]. Recently, a model that incorporates many of these features has been proposed, and numerical simulations were found in good qualitative agreement with experiments[20]. Despite this progress, direct evidence of the eventual role of strong correlation effects remained unclear. In this work we provide compelling evidence of the accumulation and depletion of oxygen vacancies as the driving mechanism of resistive switching by direct observation of the spectroscopic changes at the bare surface of PCMO in its high and low resistance states. Moreover, we also show that a large change in the electronic conductance is achieved by tuning the system to a Mott transition through hole doping control. This is done by means of voltage-induced migration of oxygen vacancies at the bare surface of the manganite.

In this study we switch the resistance of the fabricated device using a tungsten tip as a TE in direct contact with the exposed PCMO surface in air, as shown in Fig. 1(a). This enables the subsequent spectroscopic study of electronic structure changes at the bare surface[21,22].

## Results

**Resistive switching characteristics.** The I–V characteristic shown in Fig. 1(b) reveals the resistive switching effect with sudden set and reset resistive changes induced at voltages of +3.4 V and −3.3 V, respectively. The role of oxygen vacancies may be to either affect the height and/or width of the barrier, or to control the carrier concentration. For instance, in p-type oxide semiconductors, oxygen vacancies are considered to be acceptor scavengers. Therefore, a decrease in oxygen vacancy concentration at the interfaces under positive voltage may cause the depletion layer to narrow in PCMO, resulting in a decrease in the contact resistance, leading to counterclockwise I-V characteristics. In this study, the x = 0.3 in $Pr_{1-x}Ca_xMnO_3$ sample is in fact classified a p-type oxide semiconductor with a $Mn^{3+/4+}$ mixed-valence state. However, as shown in Fig. 1(b), a clockwise switching was observed. This type of I–V characteristics in p-type PCMO was previously reported in a number of studies[16,23,24], and was interpreted as due to a redox reaction at the TE. In those systems, under a positive voltage, the TE takes oxygen from the PCMO surface due to the larger free energy of the oxidation reaction of the metal. Under the opposite voltage, the reaction is reversed, and the oxidized electrode gives the oxygen ions back to the PCMO surface, leading to the clockwise effect as observed here, consistent with the relatively high oxidation free energy of the W tip. Here we shall perform the spectroscopic study of the surface in both resistive states, to investigate the effect of the redox reaction on the electronic structure of the PCMO. An important aspect of our experimental method is that it accesses the intrinsic changes in the PCMO, while it completely avoids the influence of eventual changes in the TE[21,22].

**Electronic structure of PCMO.** In order to facilitate the analysis of the spectra, Fig. 2(a) shows the schematic energy splitting for the Mn 4+ and 3+ ions. The five 3d states split into three $t_{2g}$ states and two $e_g$ states by ligand field theory in the formation of $Mn^{4+}$-O octahedron. Furthermore, each energy state splits into majority (↑) and minority (↓) spin, due to strong Hund's coupling $J_{ex}$. In the case of $Mn^{3+}$-O octahedron, one would have a single electron occupying the $e_g\uparrow$ doublet, thus leading to a metallic state. However, strong onsite Coulomb interactions favor the localization of those electrons. The ensuing entropic cost of the single electron in the doubly degenerate Mn 3d $e_g\uparrow$ state, provokes the further splitting of the levels into Mn 3d $e^1_g$ and $e^2_g$ via a Jahn-Teller (JT) distortion of the octahedron. Thus, the end compound at x = 0, $PrMnO_3$ (PMO) should have fully occupied Mn 3d $e^1_g\uparrow$ orbitals, realizing a Mott insulator state with a correlation gap driven by Coulomb repulsion and JT distortion (Fig. 2(b)). To assist our discussion, we show in Fig. 2(b) a schematic representation of the electronic structure of PCMO and PMO[25–27]. However, this diagram is only approximate, since spin, orbital, charge and lattice degrees of freedom are active in manganites, hence the precise determination of their electronic structure remains a formidable problem of strongly correlated physics[12,13]. The Mott insulator states of early or late transition metal oxides are often classified as Mott-Hubbard or charge transfer insulators. Mn is, however, an intermediate case, and the top of the O 2p and Mn 3d $e^1_g$ bands overlap in energy and are strongly hybridized. Upon chemical doping the Mott insulator, as in $Pr_{0.7}Ca_{0.3}MnO_3$, there is a mixed valance state $Mn^{3+}/Mn^{4+}$ where the holes are doped into both, the O 2p and Mn 3d $e^1_g$ bands. However, due to strong interactions, these holes do not yield a metallic state but a correlated semiconductor, with a vanishing density of states at the Fermi energy, possibly due to orbital or

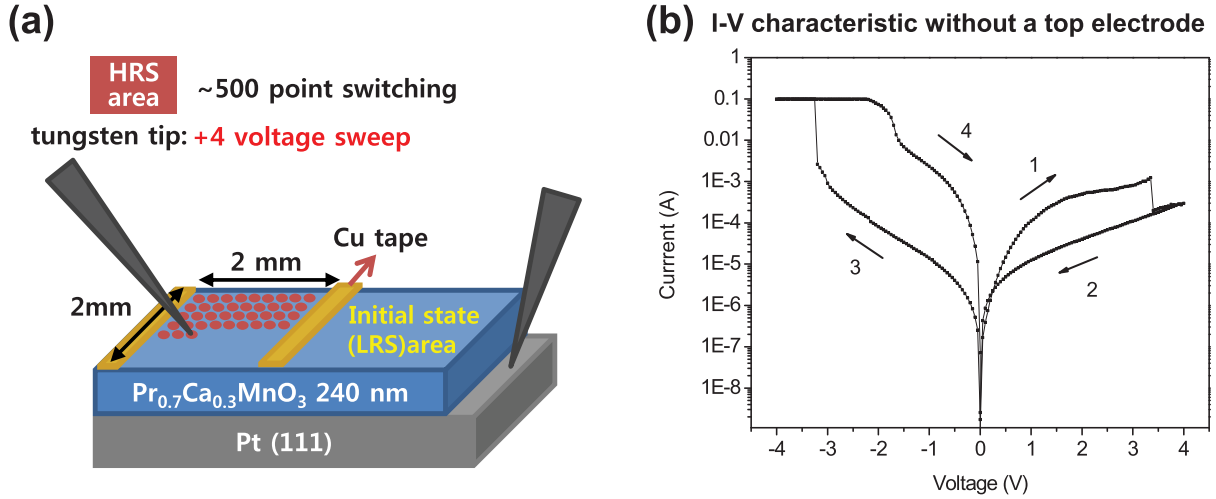


**Figure 1 | A scheme of sample preparation and the resistive switching behavior.** (a) Scheme of sample preparation for measurement. HRS and LRS regions of 2 mm × 2 mm were defined on the PCMO surface of a single sample using Cu tape. A W tip was used to switch 500 points densely distributed in the HRS region. The diameter of the tip was around 5 μm. The HRS region was switched to high resistance after the 1 and 2 sweep in the I–V characteristic, while the LRS region has already a low resistance in the initial state. (b) I–V characteristic of PCMO/Pt structure in a DC voltage sweep of ± 4 V and compliance current of 100 mA (top).

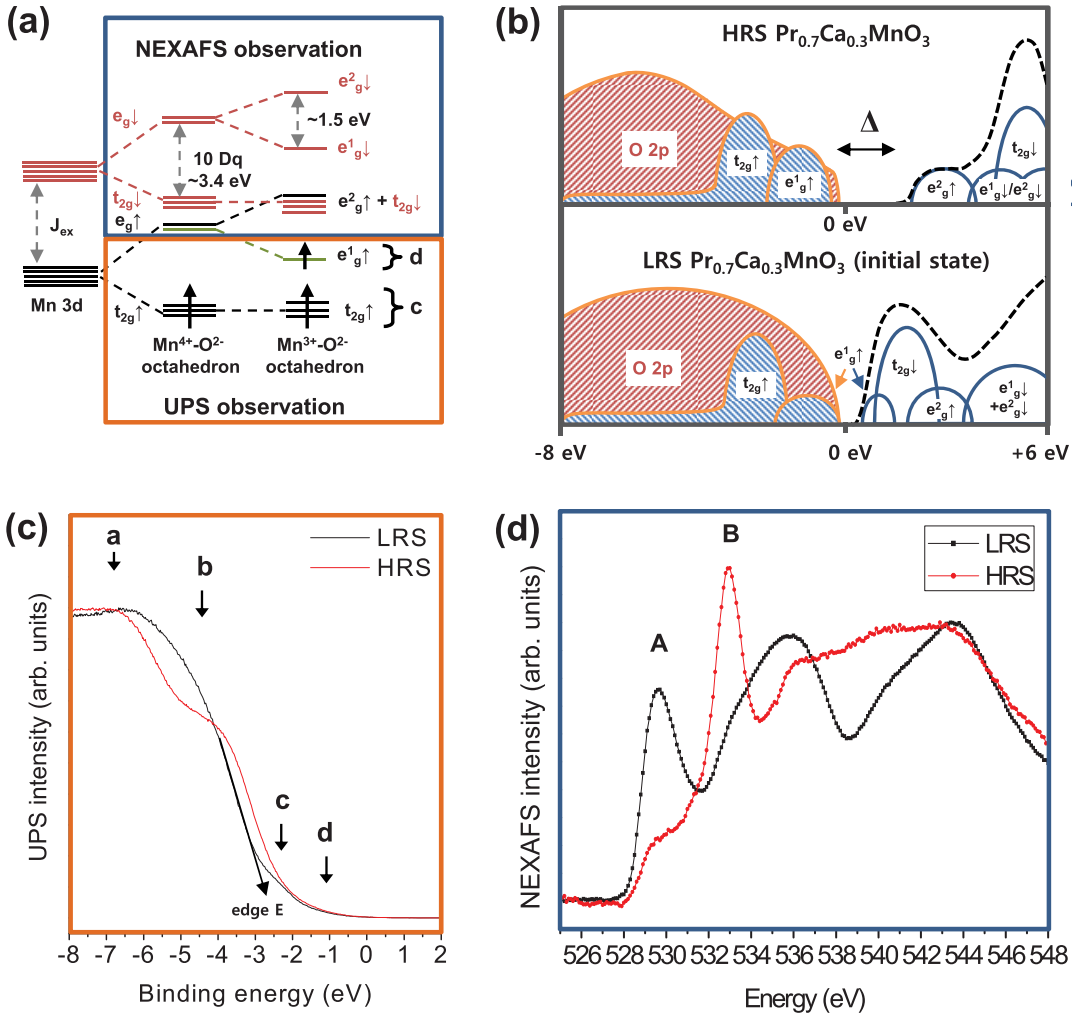


**Figure 2 | A scheme of Mn 3d electronic structure and $Pr_{0.7}Ca_{0.3}MnO_3$ band structure of LRS and HRS.** (a) The scheme of the Mn 3d electronic structure of $Mn^{3+}$-$O^{2-}$ and $Mn^{4+}$-$O^{2-}$ octahedron. The crystal field splitting (10 Dq) separates $t_{2g}$ from $e_g$ levels. In the $Mn^{3+}$-$O^{2-}$ octahedron, JT distortion further lifts the degeneracy of the $e_g$ levels. (b) A schematic of the density of states of the Mott-Hubbard insulator HRS $Pr_{0.7}Ca_{0.3}MnO_3$ (the band splitting is induced by strong correlation effects) with a gap (as would be expected for the "parent compound" $PrMnO_3$), and the hole-doped correlated semiconductor LRS $Pr_{0.7}Ca_{0.3}MnO_3$. The shaded (unshaded) part corresponds to the occupied (empty) density of states measured in the UPS (NEXAFS) spectrum. (c) The UPS data of the LRS and HRS. (d) The NEXAFS data of the LRS and HRS.

charge short-ranged order, or some other type of spatial correlations (Fig. 2(b))[28,29].

**Ultraviolet photoelectron spectroscopy and near edge x-ray absorption fine structure of HRS and LRS on PCMO surface.** Figure 2 (c) and (d) respectively show ultraviolet photoelectron spectroscopy (UPS) (valence band), and O 1s near edge x-ray absorption fine structure (NEXAFS) data of the LRS and HRS of PCMO. The UPS spectrum of the initial LRS reveals a bandwidth of approximately 10 eV, and the valence bands were labeled as **a**, **b**, **c** and **d**. They are respectively associated with contributions from: hybridization states of Mn 3d - O 2p (**a**), O 2p non-bonding states (**b**), Mn $t_{2g}\uparrow$ and Pr 4f states (**c**), and Mn 3d $e^1_g\uparrow$ states (**d**)[28,30]. Interestingly, after inducing the resistive change by electric pulsing, the UPS signal of the resulting HRS reveals significant changes. The spectrum shows a notable decrease in the intensity of the O 2p band (**b**) and an upward energy shift of the edge **E**, ie to lower binding energy, of ~0.35 eV (indicated by an arrow). Both changes are consistent with the increase of oxygen vacancies by a voltage-induced reduction, a reduced bond-binding energy from the missing O coordination, and an increase of the occupation of $e^1_g\uparrow$ states (Fig. 2(b)). On the other hand, the NEXAFS data corresponds to the absorption associated to the dipole-allowed transition where an O 1s electron is excited to unoccupied O 2p orbitals (Fig. 2(d)). The signal results from the hybridization of the O 2p orbitals with Mn, Pr and Ca. We assume that the XAS spectrum within the energy range of 526 to 535 eV is dominated by Mn 3d character, while the higher-energy region, above 535 eV, is associated to bands with Pr and Ca character[31]. In the initial LRS, the O 1s NEXAFS shows a prominent absorption peak (**A**), ascribed to the partially empty (hole doped) $e^1_g\uparrow$, and also to the fully empty $t_{2g}\downarrow$ and $e^2_g\uparrow$ bands (with $t_{2g}\downarrow$ states being the main contribution). In addition, there is an absorption peak of the Mn 3d $e^1_g\downarrow + e^2_g\downarrow$ band around 533 eV[30–33]. The comparison with the corresponding spectra measured in the HRS reveals interesting changes. The most prominent are the virtual disappearance of the feature **A** and the increase of the spectral weight of peak **B**. They are also consistent with the increase in the concentration of oxygen vacancies on the surface of the HRS. Doping by oxygen vacancies can be effectively considered to reduce the nominal hole doping of the system, as electrons are "released" by the missing oxygen ion. In fact, those electrons go to fill-up the lower-energy *empty* states of the hole doped PCMO, which are mainly the Mn 3d $e^1_g\uparrow$ just above the Fermi energy, therefore producing the decrease of the absorption peak (**A**). The second

surprising feature revealed by the HRS data is the increase in the intensity of the peak **B**. These features can be associated to the on-site Coulomb interaction $U$ due to double occupation. In fact, we note that the decrease of the absorption peak **A** appears to be rather large to be solely due to the change in occupation (ie the electronic filling-up) of $e^1_g\uparrow$ (and also $e^2_g\uparrow$ and $t_{2g}\downarrow$) states (see Fig. 2a, b and d). On the other hand, the significant increase in the intensity of peak **B** can be interpreted as due to the Coulomb shift of the $t_{2g}\downarrow$ band with weight transferred from **A**, ie is associated to the Mott gap opening phenomenon[25–27]. Moreover, the change in Mn 3d occupation is confirmed by Mn L-edge absorption (See Fig. S1 of *on-line supplementary information*). The Mn-$L_3$ and Mn-$L_2$ peaks shift to lower energy (due to chemical shift of Mn 2p) and the intensity ratio $I(L_3)/I(L_2)$ increase, consistent with a decrease of the hole carrier concentration by reduction. The intensity ratio of Mn-$L_3$ and Mn-$L_2$ indicates a valence state distribution of Mn ion in manganese oxides.

As we just argued, the systematic changes observed in the spectra of resistive switched PCMO are consistent with a voltage induced surface reduction, that is, with the increase in the concentration of oxygen vacancies in the HRS. This reduction implies a decrease in the nominal hole-doping concentration, x= 0.3. So a question that emerges is whether this decrease in the doping level may be large enough to drive the system to the Mott-Hubbard insulator state, which should occur for $Pr_{0.7}Ca_{0.3}MnO_{3-y}$, with y = 0.15, and the consequent opening of the correlation gap Δ. As we shall see next, the distribution of oxygen vacancies will be very inhomogeneous in the HRS. This may enable the system to *locally* achieve the level of concentration of oxygen vacancies (~0.15/3 = 0.05, ie 5%) that are required to reach the Mott state.

**Spectromicroscopy and NEXAFS observation: Mott gap opening.** It is well established that the RS phenomena are spatially inhomogeneous; therefore, to address the previous question we turn to an experiment aimed at exploring the spatial distribution of resistive switched regions on the sample surface. We individually switched 500 points on the surface of the sample as shown in Fig. 1(a), and subsequently performed a spectromicroscopy (SPEM) study by micro-beam NEXAFS at the locally switched regions. This is also an important crosscheck of the NEXAFS data shown in Fig. 2, as the HRS may contain spurious spectral contributions of the LRS due to the larger spot size. The SPEM image was obtained by measuring the spatial distribution of absorption of the horizontally polarized beam. The energy of the incident beam in the SPEM measurement was tuned at 529 eV to obtain a map of the distribution of the HRS and the LRS regions. The spatial resolution of the SPEM (ie, the size of the spot) was about 500 nm × 300 nm. As shown in the Fig. 3(a), the image of the sample reveals significant spatial inhomogeneity. The dark regions, with observed typical sizes of about 2~5 μm, indicate the HRS and therefore should correspond to higher concentration of oxygen vacancies. Figure 3 displays the full spectrum of O 1s NEXAFS obtained with the micro beam at two different locations, a spot inside the dark region (HRS) and one inside the bright region (LRS). As may be expected, the spectra measured within the dark and bright regions show good overall agreement with the respective HRS and LRS NEXAFS data of Fig. 2(d). We also observed, nevertheless, a significant difference in the location of the conduction band edges of the HRS and LRS of Fig. 3(b) with respect to Fig. 2(d). While in the latter case both band edges occur at about the same energy (528 eV), in the former case the HRS band edge is shifted around 0.7 eV upwards with respect to that of the LRS. The difference stems from the fact that with the local SPEM measurement we obtain the pure NEXAFS spectral contribution of solely the HRS, without "mixing" with the LRS. The shift corresponds to the observation of the clean Mott gap that we discussed before. As a further consistency check of our data, we used the NEXAFS spectra of Fig. 3(b) to simulate the HRS data of Fig. 2(d) as a linear combination of the two "pure" spectra (See Fig. S2 of *on-line supplementary information*).

## Discussion

The spectroscopic study done directly on the bare surface of PCMO allowed us to demonstrate that strong correlation effects are involved in resistive switching phenomena of this compound. Importantly, they can be of high leverage value in enhancing the switching effect, as observed in the sharp transitions of the I–V curves, with conductance jumps of more than an order of magnitude. As suggested by the analysis of our data, the transition may be due to the electric field-induced doping-control of a Mott insulator. It is important to distinguish that our doping mechanism is different low-temperature electrostatic-doping done in field effect transistor devices with a transition metal oxide channel[34]. Here the induced doping is achieved at room temperature, is non-volatile and approximately

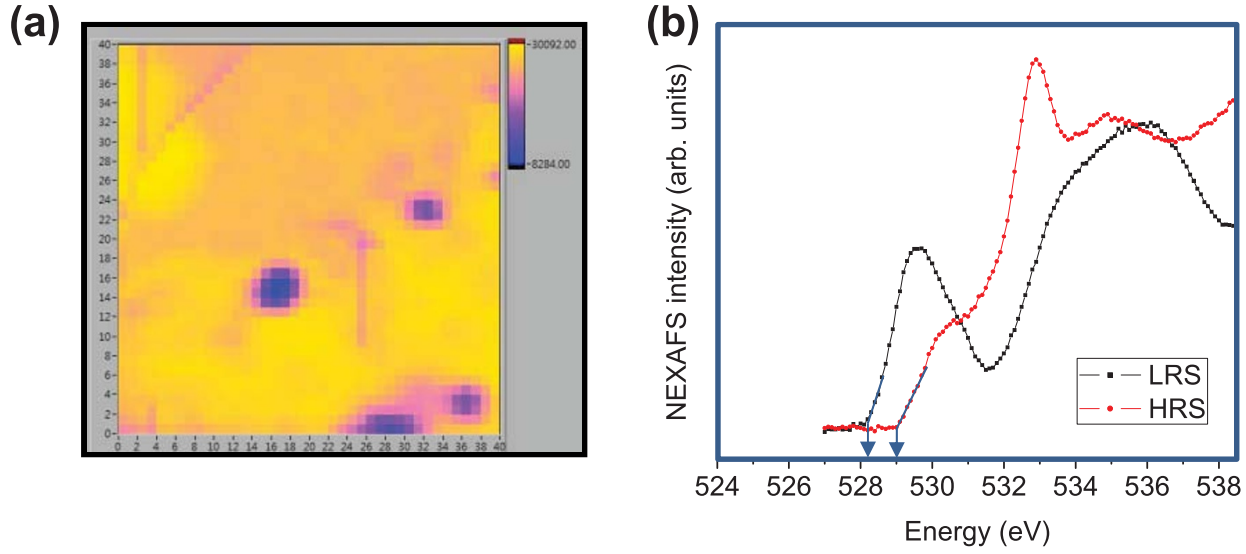


**Figure 3 | SPEctroMicroscopy image and O 1s NEXAFS on LRS and HRS region.** (a) The imaged PCMO surface by a micro-beam scan with incident energy of 529 eV. The pixel size is 1 μm × 1 μm. (b) The NEXAFS data of O 1s absorption at a spot in the dark region (HRS), and at a spot in the bright region (LRS). For reliable local area measurement, the range of energy was limited to 15 eV due to a depth of focus.

reversible. In fact, we have checked that switching the system back to the LRS gives a NEXAFS spectrum that is qualitatively similar to the initial one, however the recovery is not fully complete due to a degradation effect (See Fig. S3 of *on-line supplementary information*). This shortcoming is quite generally observed in resistive switching phenomena, and represents a potential technological problem for eventual practical applications.

Several exciting questions still remain open, for instance, whether the reduced HRS may be an orbitally or magnetically ordered state, or if it is mainly dominated by disorder. However, perhaps the most pressing issue ahead is to find out whether strong correlation effects in resistive switching of correlated transition metal oxides is a generic feature; and, in that case, whether it may be controlled and exploited to open the route for new exciting strongly correlated oxide electronic devices.

## Methods

The sample consisted in 240 nm thick film of PCMO with preferred orientation (112)/(020) fabricated by rf magnetron sputtering on a Pt(111)/Ti/$SiO_2$/Si substrate. The background pressure in the sputter chamber was lower than $1.0 \times 10^{-7}$ torr, and the deposition conditions of power, substrate temperature, deposition pressure, and Ar::$O_2$ ratio were 100 W, 500°C, 1 mtorr, and 4::1, respectively. The film thickness and the phase formation and crystallinity were confirmed by scanning electron microscopy (SEM: JSM-600F, JEOL) and X-ray diffractometry (XRD, D/MAX-2000, Rigaku) with Cu $K_\alpha$ radiation, respectively. The resistance switching behavior of the PCMO film was measured using a two-probe measurement system with an Agilent B1500A semiconductor device analyzer. All measurements were performed at room temperature.

The experimental setup is shown in Fig. 1(a). After switching the PCMO film in air, it was investigated using O 1s NEXAFS and UPS (He I radiation of 21.22 eV) in the ultra high vacuum chamber of the 8A2 beam line at Pohang Accelerator Laboratory. The NEXAFS of the PCMO film within the switched region were measured with horizontally polarized photons at a normal incidence. The measurement of UPS was performed with an incident angle of 45° and normal emission to the surface. The size of the photon beam was under 500 μm, and it was aimed at the switched region with a CCD camera and a manipulator.

The SPEM experiment was performed on the 8A1 beam-line at the Pohang light source. Monochromatized x-rays were focused with a Fresnel zone plate. The SPEM image was obtained by measuring the spatial distribution of absorption of the horizontally polarized beam. The energy of the incident beam in the SPEM measurement was 529 eV to detect the local HRS region. O 1s NEXAFS of the detected HRS region was measured by focused x-ray beam. The flux of the beam was about $10^9$ photons $s^{-1}$, and the spatial resolution of the SPEM (ie, the size of the spot) was about 500 nm × 300 nm.


1. Rozenberg, M. J. *Resistive switching.* Scholarpedia **6** (4), 11414 (2011).
2. Waser, R., Dittmann, R., Staikov, G. & Szot, K. Redox-Based Resistive Switching Memories – Nanoionic Mechanisms, Prospects, and Challenges. *Adv. Mater.* **21**, 2632–2663 (2009).
3. Sawa, A. Resistive switching in transition metal oxides. *Mater. Today* **11**, 28–36 (2008).
4. Rozenberg, M. J., Inoue, I. H. & Sanchez, M. J. Nonvolatile Memory with Multilevel Switching: A Basic Model. *Phys. Rev. Lett.* **92**, 178302–1/4 (2004).
5. Odagawa, A. *et al.* Colossal electroresistance of a $Pr_{0.7}Ca_{0.3}MnO_3$ thin film at room temperature. *Phys. Rev. B* **70**, 224403–1/4 (2004).
6. Sawa, A., Fujii, T., Kawasaki, M. & Tokura, Y. Hysteretic current–voltage characteristics and resistance switching at a rectifying Ti/$Pr_{0.7}Ca_{0.3}MnO_3$ interface. *Appl. Phys. Lett.* **85**, 4073–1/3 (2004).
7. Oka, T. & Nagaosa, N. Interfaces of Correlated Electron Systems: Proposed Mechanism for Colossal Electroresistance. *Phys. Rev. Lett.* **95**, 266403–1/4 (2005).
8. Szot, K., Speier, W., Bihlmayer, G. & Waser, R. Switching the electrical resistance of individual dislocations in single-crystalline $SrTiO_3$. *Nat. Mater.* **5**, 312–320 (2006).
9. Nian, Y. B., Strozier, J., Wu, N. J., Chen, X. & Ignatiev, A. Evidence for an Oxygen Diffusion Model for the Electric Pulse Induced Resistance Change Effect in Transition-Metal Oxides. *Phys. Rev. Lett.* **98**, 146403–1/4 (2007).
10. Kuiper, P., Kruizinga, G., Ghijsen, J., Sawatzky, G. A. & Verweij, H. Character of Holes in $Li_xNi_{1-x}O$ and Their Magnetic Behavior. *Phys. Rev. Lett.* **62**, 221–224 (1989).
11. Kuiper, P. *et al.* Unoccupied density of states of $La_{2-x}Sr_xNiO_{4+\delta}$ studied by polarization-dependent x-ray-absorption spectroscopy and bremsstrahlung isochromat spectroscopy. *Phys. Rev. B* **44**, 4570–4575 (1991).
12. Dagotto, E. *Nanoscale Phase Separation and Colossal Magnetoresistance* (Springer-Verlag, Berlin Heidelberg, 2003).
13. Bocquet, A. E., Mizokawa, T., Saitoh, T., Namatame, H. & Fujimori, A. Electronic structure of 3*d*-transition-metal compounds by analysis of the 2*p* core-level photoemission spectra. *Phys. Rev. B* **46**, 3771–3784 (1992).
14. Anisimov, V. I., Elfimov, I. S., Korotin, M. A. & Terakura, K. Orbital and charge ordering in $Pr_{1-x}Ca_xMnO_3$ (x=0 and 0.5) from the ab initio calculations. *Phys. Rev. B* 55, 15494–15499 (1997).
15. Lee, D. H. *et al.* Atomic structure of conducting nanofilaments in $TiO_2$ resistive switching memory. *Nat. Nanotechnol.* **5**, 148–153 (2010).
16. Li, S. L., Shang, D. S., Li, J., Gang, J. L. & Zheng, D. N. Resistive switching properties in oxygen-deficient $Pr_{0.7}Ca_{0.3}MnO_3$ junctions with active Al top electrodes. *J. Appl. Phys.* **105**, 033710–1/6 (2009).
17. Akinaga, H., Shima, H. ReRAM technology; challenges and prospects. *IEICE Electron. Express* **9**, 795–807 (2012).
18. Hasan, M. *et al.* Uniform resistive switching with a thin reactive metal interface layer in metal-$La_{0.7}Ca_{0.3}MnO_3$-metal heterostructures. *Appl. Phys. Lett.* **92**, 202102–1/3 (2008).
19. Dong, R. *et al.* Improvement of reproducible hysteresis and resistive switching in metal-$La_{0.7}Ca_{0.3}MnO_3$-metal heterostructures by oxygen annealing. *Appl. Phys. Lett.* **90**, 182118–1/3 (2007).
20. Rozenberg, M. J. *et al.* Mechanism for bipolar resistive switching in transition-metal oxides. *Phys. Rev. B* **81**, 115101–1/5 (2010).
21. Asanuma, S., Akoh, H., Yamada, H. & Sawa, A. Relationship between resistive switching characteristics and band diagrams of Ti/$Pr_{1-x}Ca_xMnO_3$ junctions. *Phys. Rev. B* **80**, 235113–1/8 (2009).
22. Yasuhara, R., Yamamoto, T., Ohkubo, I., Kumigashira, H. & Oshima, M. Interfacial chemical states of resistance-switching metal/$Pr_{0.7}Ca_{0.3}MnO_3$ interfaces. *Appl. Phys. Lett.* **97**, 132111–1/3 (2010).
23. Liao, Z. L. *et al.* Categorization of resistive switching of metal-$Pr_{0.7}Ca_{0.3}MnO_3$-metal devices. *Appl. Phys. Lett.* **94**, 253503–1/3 (2009).
24. Lee, J. M. *et al.* The impact of Al interfacial layer on resistive switching of $La_{0.7}Sr_{0.3}MnO_3$ for reliable ReRAM applications. *Microelectron Eng.* **86**, 1933–1935 (2009).
25. Satpathy, S., Popović, Z. S. & Vukajlović, F. R. Electronic Structure of the Perovskite Oxides: $La_{1-x}Ca_xMnO_3$. *Phys. Rev. Lett.* **76**, 960–963 (1996).
26. Jung, J. H. *et al.* Determination of electronic band structures of $CaMnO_3$ and $LaMnO_3$ using optical-conductivity analyses. *Phys. Rev. B* **55**, 15489–15493 (1997).
27. Yang, Z., Huang, Z., Ye, L. & Xie, X. Influence of parameters *U* and *J* in the LSDA+*U* method on electronic structure of the perovskites $LaMO_3$(M=Cr,Mn,Fe,Co,Ni). *Phys. Rev. B* **60**, 15674–15682 (1999).
28. Ebata, K. *et al.* Chemical potential shift and spectral-weight transfer in $Pr_{1-x}Ca_xMnO_3$ revealed by photoemission spectroscopy. *Phys. Rev. B* **74**, 064419–1/6 (2006).
29. Wadati, H. *et al.* In Situ Photoemission Study of $Pr_{1-x}Ca_xMnO_3$ Epitaxial Thin Films with Suppressed Charge Fluctuations. *Phys. Rev. Lett.* 100, 026402–1/4 (2008).
30. Saitoh, T. *et al.* Electronic structure of $La_{1-x}Sr_xMnO_3$ studied by photoemission and x-ray-absorption spectroscopy. *Phys. Rev. B* **51**, 13942–13951 (1995).
31. Abate, A. *et al.* Controlled-valence properties of $La_{1-x}Sr_xFeO_3$ and $La_{1-x}Sr_xMnO_3$ studied by soft-x-ray absorption spectroscopy. *Phys. Rev. B* **46**, 4511–4519 (1992).
32. Kurata, H. & Colliex, C. Electron-energy-loss core-edge structures in manganese oxides. *Phys. Rev. B* **48**, 2102–2108 (1993).
33. Dalai, M. K. *et al.* Electronic structure of $Pr_{0.67}Ca_{0.33}MnO_3$ near the Fermi level studied by ultraviolet photoelectron and x-ray absorption spectroscopy. *Phys. Rev. B* **74**, 165119–1/6 (2006).
34. Ueno, K. *et al.* Discovery of superconductivity in $KTaO_3$ by electrostatic carrier doping. *Nat. Nanotech.* **6**, 408–412 (2011).


## Acknowledgements

This work was supported by SK Hynix Inc. of Korea and by the second stage of the Brain Korea 21 project in 2010. The experiments at the PLS were supported in part by MEST and POSTECH.

## Author contributions

H.S.L. conceived the idea and designed the experiments, and performed the sample fabrication, characterization, spectroscopy measurements with the analysis. H.S.L. and S.G.C. performed SPEM experiment. H.H.P. and M.J.R. supervised the experiments, analysis and manuscript. All authors discussed the progress of research and reviewed the manuscript.

## Additional information

**Supplementary information** accompanies this paper at http://www.nature.com/scientificreports

**Competing financial interests:** The authors declare no competing financial interests.



**How to cite this article:** Lee, H.S., Choi, S.G., Park, H.-H. & Rozenberg, M.J. A new route to the Mott-Hubbard metal-insulator transition: Strong correlations effects in $Pr_{0.7}Ca_{0.3}MnO_3$. *Sci. Rep.* **3**, 1704; DOI:10.1038/srep01704 (2013).